

A Time Resolved Study of Precoated AISI 441 for SOFC Interconnects using STEM-EELS – Part I

L. S. Karlsson^a, M. W. Lundberg^b, R. Berger^b, and J. Westlinder^b

^a Physical Metallurgy, AB Sandvik Materials Technology, 81181 Sandviken, Sweden

^b Surface Technology, AB Sandvik Materials Technology, 81181 Sandviken, Sweden

Precoated AISI441 for SOFC interconnectors were investigated by STEM-EELS looking at the diffusion processes in the initial stage of the oxidation. The electron beam physical vapour deposition (EB-PVD) coating contained Ce and Co/Mn-alloy in two layers with a total thickness of 800 nm. The samples were exposed up to 1000 hours at 800°C, and then characterized by STEM-EELS. Multiple linear least squares (MLLS) fitting of reference spectra aids the interpretation of the elemental maps due to overlapping edges. Within 4 min heat treatment the oxidation front has reached the substrate steel and Cr₂O₃ is forming at the stainless steel interface. CeO₂ acts as the barrier line for Cr and is situated between the Cr-containing spinels and the (Co,Mn)-spinel after up to 168 h heat treatment.

Introduction

A solid oxide fuel cell (SOFC) is an electrochemical device which converts chemical energy in fuels into electrical energy. The fuel cell is containing an electrolyte sandwiched between a porous anode and a porous cathode. The fuel cell is then separated from the next by interconnects building up the SOFC stack. Today, most interconnects for SOFC are metallic and based on ferritic stainless steels. The properties that are the most important are high electronic conductivity, a thermal expansion coefficient similar to the surrounding adjacent ceramic components, and a thermal stability at service temperatures roughly spanning from 550°C to 1000°C. Water is a byproduct of the electrochemical conversion and thus an oxidation resistant material is required for the interconnector. Among the ferritic stainless steel candidates (alumina, chromia, or silica) only chromia formers are suitable as both alumina and silica form insulating protective scales (1,2). Steel producers and other developers have developed alloys with an expected lifetime of 40,000 hours, a coefficient of thermal expansion compatible with the ceramic components of SOFCs, good surface conductivity in the formed oxide scale etc. However, the specialized interconnector steel grades are still costly to manufacture due to the alloying elements and production routes and as a result, other ferritic stainless steel grades spanning from AISI430 to 446 have been considered.

Sandvik Materials Technology have been developing interconnector steels and surface coatings for interconnect steels for more than a decade. Co coatings, for instance, can be used to minimize detrimental chromium evaporation from ferritic stainless steel and to improve the electrical conductivity of the formed oxide scale (3). The idea is to deposit a metallic Co coating which will oxidize and react with Mn that diffuses from the

substrate to the Co coating, resulting in a CoMn-spinel at the surface on the interconnect. Except from substantially reducing the Cr evaporation (3) the formed CoMn-spinel will have a relatively good electrical conductivity (4). The thickness of the CoMn-spinel will be dependent of the initial thickness of the Co coating and it has been shown that up to a cobalt thickness around 600-800 nm the Cr evaporation is suppressed linearly with Co layer thickness. It has been shown that a small amount of Ce added to the spinel improves the ASR as well as reduces the mass gain due to less oxidation (5). Although the effect of the additional Ce layer is evident, the mechanism is not fully understood. Earlier studies (5,6) within the EU FP7 METSOFC project performed at Chalmers University of Technology have shown that nanocoatings of this type strongly decreases the oxidation rate and therefore improves the long term stability of the interconnect.

A time resolved study of Ce/Co-Mn coated AISI 441/OC365 strip steel intended for interconnects in solid oxide fuel-cells (SOFC) has been conducted within SMT R&D. In this study the combination of scanning transmission electron microscopy (STEM) and electron energy loss spectroscopy (EELS) is utilised for advanced materials characterisation in collaboration with the Kelvin Nanocharacterisation Centre, Glasgow University. As the amount of data collected is quite huge we have decided to divide the results into two papers for clarity and the readers benefit. However, we recommend reading the papers side by side.

Experimental

Cold rolled steel strip with a thickness 0.2 mm of a commercial ferritic stainless steel AISI441 were used in the present study. The nominal chemical composition is (in wt%): 17.8 Cr, 0.48 Nb, 0.26 Mn, 0.55 Si, 0.01, Ni 0.013, Ti 0.139. Closest to the stainless steel surface a 10 nm cerium layer was deposited by electron beam physical vapor deposition (EB-PVD) in a laboratory batch coater followed by a 600 nm thick co-evaporated manganese cobalt layer. The target value for the composition was 1:2 for the first 400 nm and then reversed, 2:1, for the remaining 200 nm, this to investigate the process control as well as to investigate how different areas diffuse after cyclic oxidation. Before coating deposition all substrates were cleaned in acetone and ethanol followed by alkaline cleaning at 60°C for 10 min. After alkaline cleaning the substrates were rinsed in hot tap water, deionized water and finally in ethanol. The uncoated substrates were cleaned in the same way before the oxidation experiments. The size of the double sided coated substrates was 15×30 cm. Sample coupons were cut with the dimensions 15 mm × 15 mm. A hole with 3 mm in diameter was punched into the sample for sample handling. Before exposure the samples were degreased and cleaned as previously described. The samples were mounted vertically on an alumina sample holder, and positioned parallel to the gas flow, in the center of a horizontal tube furnace. The furnace was operated at 800°C. The reaction gas consisted of 20% O₂, 77% N₂ and 3% H₂O. The volumetric flow rate was 1000 ml/minute, giving a linear flow rate of approximately 3.8 cm/s. Digital mass flow controllers were used for the dry carrier gases. For adding the water vapor, the dry gas flow was bubbled through a humidifier and cooled to the correct dew point (24.4°C for 3% water vapor) in a condenser, before being led into the furnace. All parts of the system downstream of the condenser were kept above the relevant dew point, in order to prevent condensation. One sample at 72 hours and 168 hours were prepared. The sample exposed for 30 s was prepared by putting the sample in a muffle furnace in ambient air for 30 seconds for practical reasons.

The samples were subjected to heat treatment at 800°C using certain time intervals with the moment the sample were put into the furnace as the starting point. After heat treatment the samples were prepared for TEM by FIB lift-out techniques using Pt as a protective surface layer subsequently mounted on Omniprobe grids. In this study the samples subjected to 30 s, 4 min, 72 h and 168 h heat treatment were characterised.

Data acquisition

STEM-EELS data cubes were acquired on the JEM-ARM200F at the Kelvin Nanocharacterisation Centre using a 200 kV beam with 0.1-1 nm probe size with simultaneous low-loss and core-loss acquisition also known as dual-EELS mode. Reference images were acquired using the high-angular annular dark-field (HAADF) detector to generate images with atomic number (Z) contrast. In these reference images the area for the 3D data cube and drift correction were assigned before acquisition.

Data processing – Part I

After acquisition the data-sets were corrected using a fresh dark reference to compensate for any change in background caused by the intensity of the acquired spectra on the CCD. Before further analysis energy drift was corrected for using the zero-loss peak (ZLP) in the low-loss spectrum image (SI) and the O-K edge in the core-loss SI. Any thickness related effects were removed by deconvolution using the ratio method in order to remove the plural scattering in the EELS data. After this, x-rays were removed from the volume of the deconvoluted SI. Elemental maps were extracted using the dynamic map option with carefully selected background and signal windows to match the conditions of the full region of interest as closely as possible. Due to overlapping of neighbouring peaks this was not always successful and multiple-linear least-squares (MLLS) fitting to reference spectra with known peaks were performed. In this case, an energy window (575 - 920 eV) including all the peaks of interest (Table I) was chosen using reference spectra from the EELS-atlas (Cr, MnO₂, CoO and CeO₂). Ideally, the reference spectra should be acquired using materials of known composition and thickness at similar acquisition conditions but at this point all of the materials were not available to us and reference spectra from the EELS-atlas was used.

TABLE I. EELS-edges of interest in the MLLS-fitting.

Element	L₃-edge	L₂-edge
Cr	575	584
Mn	640	651
Co	779	794

Data processing – Part II

Further data analysis was done by calculating multivariate histograms from dynamic maps or MLLS fit coefficients to identify areas of specific phases. This technique can often identify regions of compositional correlation not necessarily detectable by eye. Finally, the white-line ratio of the different phases was determined from the extracted

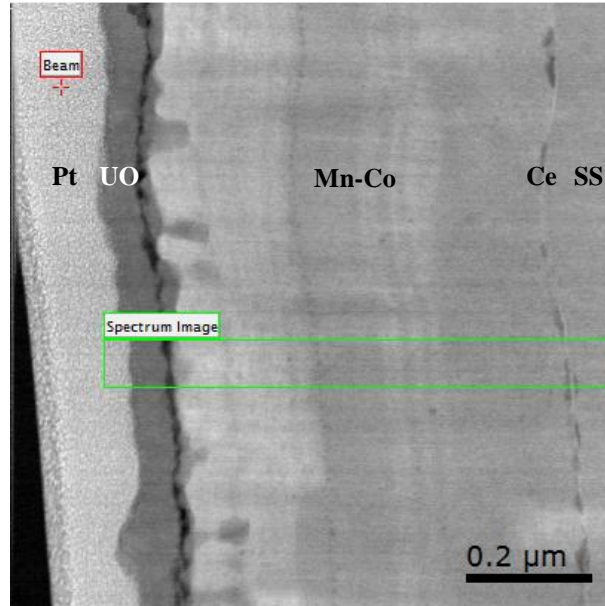
EELS-spectrum of a given phase identified by the trivariate histogram. The white line ratio could be determined using the *Double Atan EELS Background* script (7) method or the second derivative method depending on the method used in the reference literature (8,9).

Results and discussion

30 s

After 30 s heat treatment the oxidation front has reached 55 nm into the layered structure with protrusions visible at certain locations (Figure 1). The Ce layer is intact at the steel interface and Cr is mainly present in the substrate steel. The elevated levels of Cr in the Pt capping layer, upper oxide and Ce layer is most likely an artefact of the MLLS-fitting as neither Pt nor Ce was present in the reference spectra used from the EELS atlas and have peaks available in the energy range used for the fitting. The MLLS fit coefficient of MnO_2 and CoO are complementary with a Co rich section in the upper part and a Mn rich section in the lower part of the layered structure. These variations are caused by off-set of the evaporation from the Mn and Co sources plus the fact that the growth process is interrupted at certain intervals to check the growth rate. The upper oxide layer (UO) includes a layer of dark contrast that is rich in C, most likely dirt and dust deposited on the coated steel before the sample was put into the furnace for the heat treatment. The high-contrast clusters seen in the HAADF-image are likely to be redeposited Pt from the sample preparation by FIB and most likely causes the artifact of elevated Cr in the upper oxide.

02_30 s



Cr

CoO

MnO₂

CeO₂

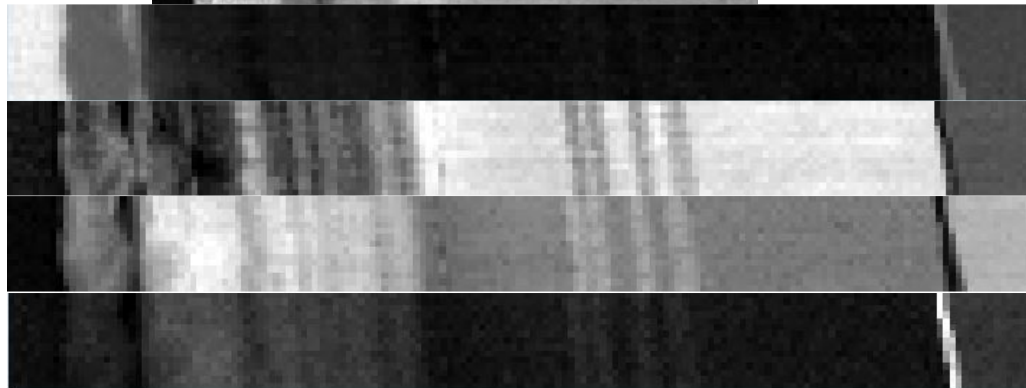


Figure 1. MLLS fit coefficient maps of Cr, MnO₂, CoO and CeO₂ for the entire coated stainless steel after 30 s heat treatment. The upper oxide (UO) formation has started at the top of the coating with protrusions into the underlying layers.

4 min

After 4 min heat treatment the oxidation front has reached all the way to the steel substrate and Cr evaporation from the steel substrate has started resulting in a 30 nm CrO_x layer at the interface (Figure 2). An 8 nm Ce-rich layer is situated above the CrO_x and the coating Co-Mn layer show a similar complementary composition in the CoO and MnO₂-fit coefficient maps as was observed after 30 s heat treatment (not shown here). Note that the interface region at the steel substrate shows an enrichment of Mn under the CrO_x layer. This interface layer could well be explained by an inclined surface between the substrate steel and the oxidized coating layers. The interfaces are often not perfectly sharp and follow the contour of the substrate steel as is evident from the overview image of Figure 2.

03_4 min

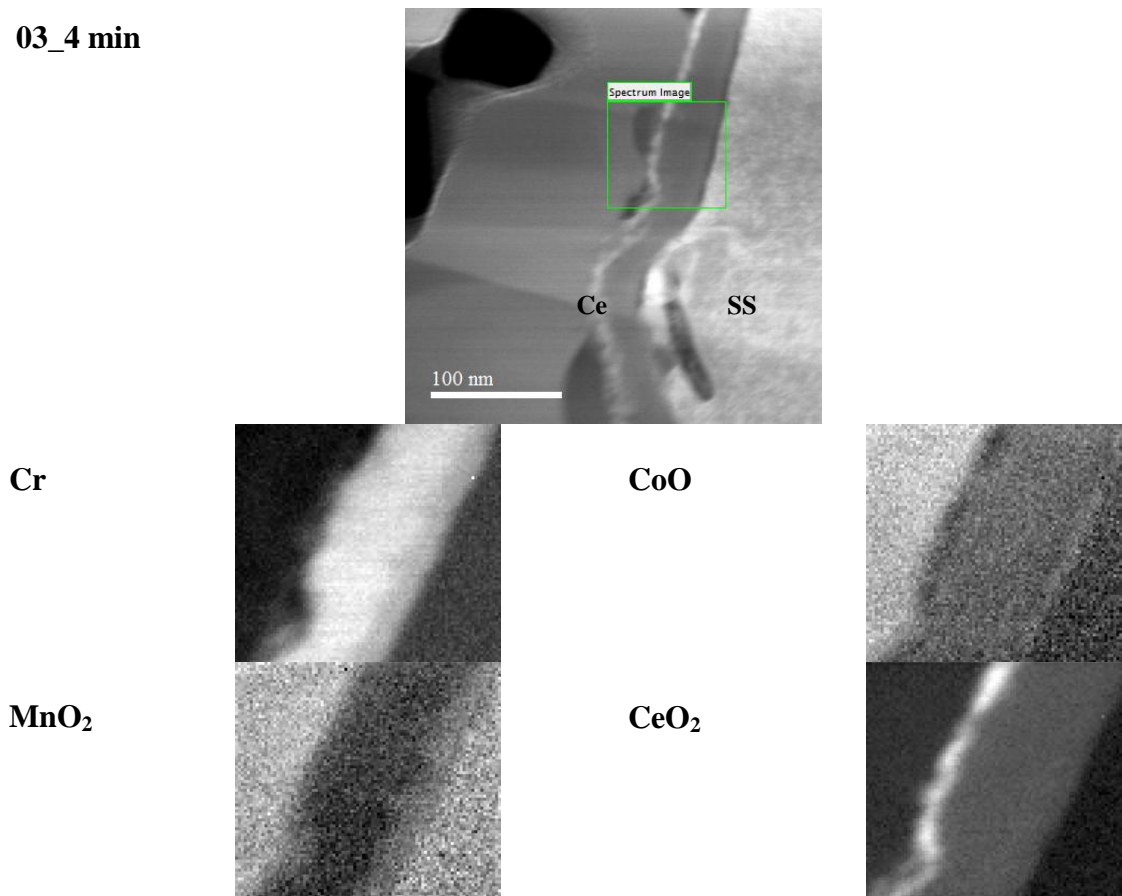
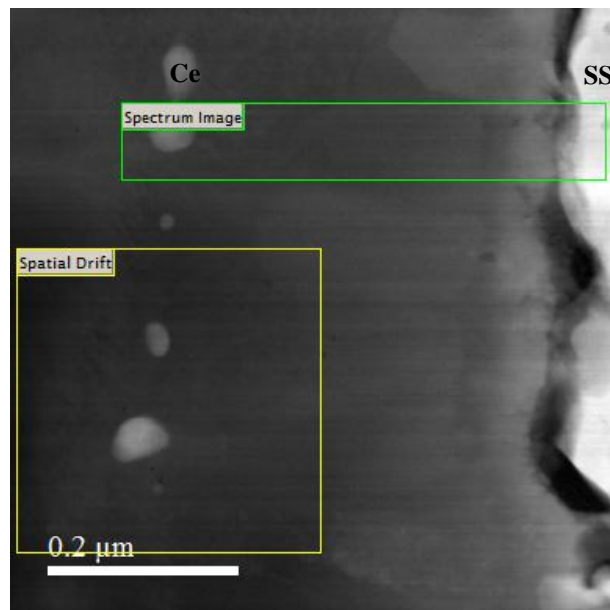


Figure 2. MLLS fit coefficient maps of Cr, MnO₂, CoO and CeO₂ for the region from the substrate steel (SS) to the Ce layer after 4 min heat treatment.

72 h

After 72 h heat treatment the Cr-front has migrated some 400 nm from the stainless steel interface and coincides with a band of discrete CeO₂-particles, as have been confirmed by high-resolution TEM (HRTEM) (10), in two size fractions; 15 or >70 nm (Figure 3). The CrO_x-layer is followed by a (Co,Cr)-spinel with a gradual increase in Mn-content until the (Co,Mn)-spinel is reached above the band of CeO₂-particles. It is clear that a reaction with the coating Co/Mn-layers has occurred and that the proximity of the Co layers in the original coating results in a transition phase of (Co,Cr)-spinel. The evaporation of Cr is therefore reduced but not fully controlled until the (Co, Mn)-spinel has formed. A perfect 50:50 Co:Mn coating would most likely control the Cr evaporation to an even larger extent. Moreover, the MnO₂ fit coefficient map shows elevated levels of Mn in the grain boundaries of the (Co,Cr)-spinel, indicating that we have Mn evaporation from the steel substrate. If the transport occurs predominantly in the grain boundaries this can be reduced by increasing the grain size as is to be expected with time as the scale grows.

02_72 h



Cr



MnO₂



CoO



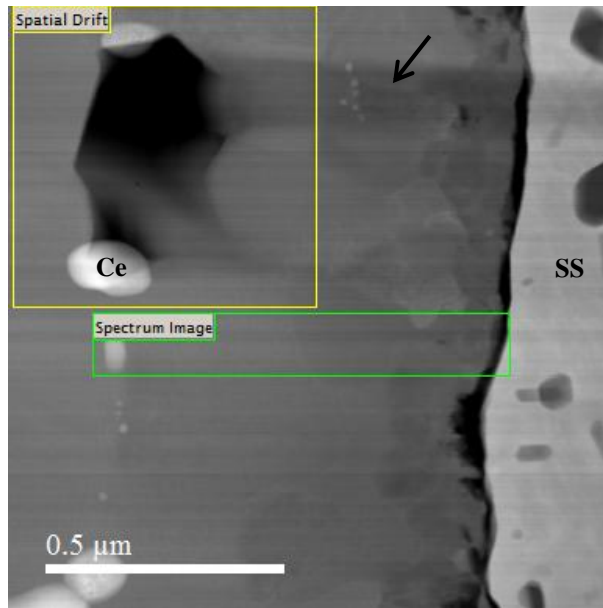
CeO₂



Figure 3. MLLS fit coefficient maps of Cr, MnO₂, CoO and CeO₂ for the region from the substrate steel (SS) to the band of CeO₂ particles after 72 h heat treatment
168 h

After 168 h heat treatment the Cr-front has reached 950 nm from the steel substrate and still coincides with a band of CeO₂-particles of two different sizes; 15 and >70 nm i.e. precisely like after 72 h heat treatment. The Ce-front coincides with the Cr-front with the CrO_x-layer being followed by a layer of (Co,Cr)-spinel gradually changing into a (Co,Mn)-spinel with increasing content of Mn (Figure 4). Interestingly, the transition phase (Co,Cr)-spinel still remains and the CrO_x and the (Co,Cr)-spinel has grown. It is clear that Cr is mobile in the system but is replaced by Mn at a certain level. As for 72 h heat treatment the Mn levels is somewhat enhanced in the grain boundaries of the (Co,Cr)-spinel but is less pronounced in this case.

05_168 h



Cr



MnO₂



CoO



CeO₂



Figure 4. MLLS fit coefficient maps of Cr, MnO₂, CoO and CeO₂ for the region from the steel substrate to the CeO₂-layer after 168 h heat treatment. The arrow indicates Ce rich particles formed by redeposition of sputtered material from a larger CeO₂-particle in the sample preparation process.

Conclusions

In this time resolved study the oxidation front and diffusion of elements can be followed after heat treatment at 800°C. Also, the observation of a (Co,Cr)-oxide layer between the Cr-oxide at the steel interface and the (Co,Mn)-oxide at the upper surface is clearly distinguishable when comparing the Cr, Co and Mn maps. With increasing heat treatment time the Cr-oxide and (Co,Mn)-oxide layers increase in thickness but the (Co,Cr)-oxide layer thickness tend to be stable.

The use of STEM-EELS and MLLS-fitting is a very powerful combination for recording local changes in composition during a time resolved study. However, for regions containing elements that are not accounted for in the MLLS-fitting routine (e.g. Pt in Figure 1) artefacts might occur. It is therefore very important to perform the data processing with care and not to over interpret the result before all other options have been ruled out. In this case the EELS Atlas reference spectra proved very useful as we wanted to study the effects of diffusion of the present elements, in particular Cr, Mn and Co. It is clear that by coating the steel with a (Co,Mn)-coating we are able to reduce the evaporation of Cr and Mn from the steel itself and therefore reduce the risk of embrittlement of the interconnect and in the long run increase the life time of the fuel cell stack. Also, if the precoated interconnect is to be used at temperatures lower than 800°C the Mn diffusion rate from the steel will decrease with lowered temperature. This could be a factor to be considered in the formation of the (Co,Mn)-spinel if the coating does not include Mn and only Co from the start.

Finally, we have showed it is possible to create and vary the composition of co-evaporated (Co,Mn)-alloy layer using EB-PVD in a laboratory scale setup. This could be used for more complex precoated layer structures for SOFC interconnects, which could be used to tailor-make the coatings based on e.g. operating temperature requirements.

Acknowledgments

The research leading to these results has received funding from the Europeans Union's Seventh Framework Programme (FP7/2007-2013) for Fuel Cells and Hydrogen Joint Technology initiative within the project METSAPP, grant agreement n° [278257] 10, and within the project NELLHI, Grant Agreement n° [621227]. The authors would also like to acknowledge the Kelvin Nanocharacterisation Centre, Glasgow University.

References

1. N. Shaigan, W. Qu, D. G. Ivey and W. Chen, *J. Power Sources*, **195**, 1529 (2010)
2. J. W. Fergus, *Mater. Sci. Eng. A*, **A397**, 271 (2005).
3. N. Shaigan, PhD Thesis, University of Alberta 2009, <http://hdl.handle.net/10048/402>.
4. U. Bexell, M. Schuisky, H. Ravash, J. Froitzheim, J.-E. Svensson, Proc. of the 9th European SOFC Forum, Lucerne, Switzerland, 29 June-2 July 2008.
5. S. Canovic, J. Froitzheim, R. Sachitanand, M. Nikumaa, M. Halvarsson, L.-G. Johansson and J.-E. Svensson, *Surface and Coatings Technology*, **215**, 62 (2013).
6. J. Froitzheim, S. Canovic, M. Nikumaa, R. Sachitanand, L.G. Johansson and J. E. Svensson *J. of Power Sources*, **220**, 217 (2012).
7. D.R.G. Mitchell. *Double Atan EELS Background*. 20121124 v1.0 Available from: http://www.dmscripting.com/double_atan_eels_background.html.
8. T. L. Daulton and B. J. Little, *Ultramicroscopy*, **106**, 561 (2006).
9. Z. L. Wang, J. S. Yin, and Y. D. Jiang, *Micron*, **31**, 571 (2000).
10. M. W. Lundberg, L. S. Karlsson, R. Berger, N. Folkesson, J. Westlinder, and B. Holmberg Proc. Of the 13th European SOFC Forum, Okinawa, Japan, 6-11 October 2013.